



HAL
open science

Generation of Virtual Microstructures of Energetic Materials Based on Micro-computed Tomography Images Analysis

Élodie Kaeshammer, Petr Dokládál, François Willot, Steve Belon, Lionel Borne

► **To cite this version:**

Élodie Kaeshammer, Petr Dokládál, François Willot, Steve Belon, Lionel Borne. Generation of Virtual Microstructures of Energetic Materials Based on Micro-computed Tomography Images Analysis. 50th International Annual Conference of the Fraunhofer ICT, Jun 2019, Karlsruhe, Germany. hal-02139566

HAL Id: hal-02139566

<https://hal.science/hal-02139566>

Submitted on 24 May 2019

HAL is a multi-disciplinary open access archive for the deposit and dissemination of scientific research documents, whether they are published or not. The documents may come from teaching and research institutions in France or abroad, or from public or private research centers.

L'archive ouverte pluridisciplinaire **HAL**, est destinée au dépôt et à la diffusion de documents scientifiques de niveau recherche, publiés ou non, émanant des établissements d'enseignement et de recherche français ou étrangers, des laboratoires publics ou privés.

GENERATION OF VIRTUAL MICROSTRUCTURES OF ENERGETIC MATERIALS BASED ON MICRO-COMPUTED TOMOGRAPHY IMAGES ANALYSIS

Kaeshammer Elodie^{1,2,3}, Dokladal Petr¹, Willot François¹, Belon Steve², Borne Lionel³

¹ CMM (Center for Mathematical Morphology) MINES-ParisTech, 35 rue St-Honoré, 77300 Fontainebleau, France ;

² CEA, DAM, CEA-Gramat, 46500 Gramat, France ;

³ ISL (french-german research Institute of Saint-Louis), PO Box 70034-F68301 Saint-Louis Cedex France

Abstract

Impact experiments were performed at the french-german research Institute of Saint-Louis on three energetic materials composed of 70 % in weight of RDX particles embedded in a wax matrix. These materials differ by the microstructural properties of the explosive particles. The experimental results reveal that the detonation thresholds, and so the sensitivity to shock, are different for each sample. To better understand these results, we characterize the microstructural properties of these compositions.

The microstructures of the three materials are imaged with micro-computed tomography (μ CT) at CEA Gramat. First, the 3D μ CT images are filtered and segmented. Then, an analysis of the segmented volume is performed (granulometry, covariance and weight fraction). Each labeled grain is extracted and characterized by several descriptors such as volume, surface, angularity, sphericity or intra-granular porosity.

Virtual microstructures are generated with the extracted grains. Each grain is precisely selected depending on its properties to generate a controlled microstructure. This allows to modify only one microstructural parameter at a time. The virtual microstructures are built to be consistent with the global analysis of the μ CT segmented volumes. They respect both morphological granulometry and spatial covariance of the μ CT segmented volumes. These numerical materials are intended to be used in mesoscale finite element simulations to study the effects of the microstructure on the shockwave propagation.

Introduction

New energetic materials tend to be less sensitive in order to increase safety. They have to better resist both thermal and mechanical aggressions. One way to reduce the sensitivity to shock of a material is to change its microstructure. The hot spot theory is commonly used to describe the initiation after an impact of an energetic material [1]. The principle is the following: the interaction of shock waves with the heterogeneities of the microstructure generates localized elevations of temperature and pressure. These areas with higher temperatures are called hot spots. In these localized zones, the temperature can exceed the reactivity threshold. The chemical reaction starts locally. The growth and coalescence of the hot spots can lead to the full detonation of the material.

The formation of hot spots, and so the sensitivity to shock, strongly depends on the microstructure. Several experimental studies investigated the role of the shape [2] and the size [3] of the explosive grains in the formation of hot spots. The role of intra-granular [4, 5, 6] and extra-granular porosities [7] were also highlighted.

The mechanisms identified which can lead to the formation of hot spots are: pore collapses [8], plastic deformations, fracture of the explosives grains or frictions between the grains [9]. Shock reflections can also create hot spots [10].

The long term objective of this study is to better understand and quantify the influence of each microstructural parameter on the formation of hot spots. This will allow to evaluate the sensitivity to shock

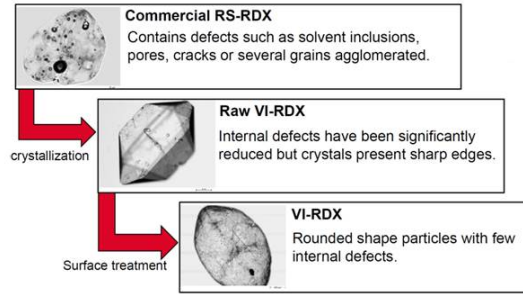


Figure 1: Formulation steps of the VI-RDX

of an energetic material knowing its microstructure.

Three materials provided by the french-german research Institute of Saint-Louis (ISL) are studied. They are composed of 70 % in weight of RDX and 30 % of a wax binder. The composition of the three materials is the same but the type of RDX, and so the microstructures, are different. The first material is made of RS-RDX from Eurenco. The grains contain numerous intra-granular defects like porosities, solvent inclusions or micro-cracks. The second material is composed of raw VI-RDX. The raw VI-RDX particles are obtained after a recrystallization of the RS-RDX grains. The recrystallization process reduces the number of internal defects but the crystals have now sharp edges. A final step of surface treatment gives the patented VI-RDX [11] with rounded grains. The third sample is made of VI-RDX (Fig. 1).

The three materials have different shock sensitivity. In previous work, ISL performed measurements of the sustained shock sensitivity with a small projectile impact experiment [5]. The VI-RDX/Wax material detonates at the highest pressure (7.2 GPa). Both raw VI-RDX and RS-RDX based materials detonate for pressure around 6.2 GPa despite noticeable microstructure differences. It is supposedly due to two competitive factors which influence the formation of hot spots: the sharp edges of the raw VI-RDX grains and the numerous intra-granular defects of the RS-RDX grains. These experiments revealed the role of the shape of the explosive grains and the intra-granular defects. But real microstructures are complex and we presumably miss the influence of other microstructural parameters (surface texture of grains, contact points between the grains, debonding effects...).

The study is divided into two steps to better understand the experimental results: i) a precise analysis of the three materials microstructures thanks to micro-computed tomography (μ CT), ii) the study of the sensitivity to shock of virtual microstructures. With virtual materials, we have a fine control on the microstructure. We are able to uncorrelate some microstructural factors (for instance the size of the grains and the number of intra-granular porosities) and better understand their role on the formation of hot spots.

The objective of this paper is to present the methodology to build controlled virtual microstructures with the RSA method. The microstructures are generated with real grains extracted from μ CT images. The first section presents the 3D microstructures of the three materials and their segmentations with the tool SAMG [12]. The segmentation is validated with a comparison between experimental acquisitions (weight fraction, diameters and bulk densities distributions) and image analysis results. The next section introduces the descriptors used to characterize each extracted grain with a focus on the definition of a new definition of the angularity index. The third section presents the methodology to build controlled virtual microstructures with the RSA method and the library of grains. The generated materials have new microstructural properties which means that some microstructural properties (for instance the sphericity or the angularity of the grains) are different than the ones of the real μ CT material. This is obtained by choosing precisely the grains from the library of extracted grains used to generate the virtual microstructures. In the last section, the representativeness of the virtual materials is evaluated with two descriptors: the granulometry and the spatial covariance.

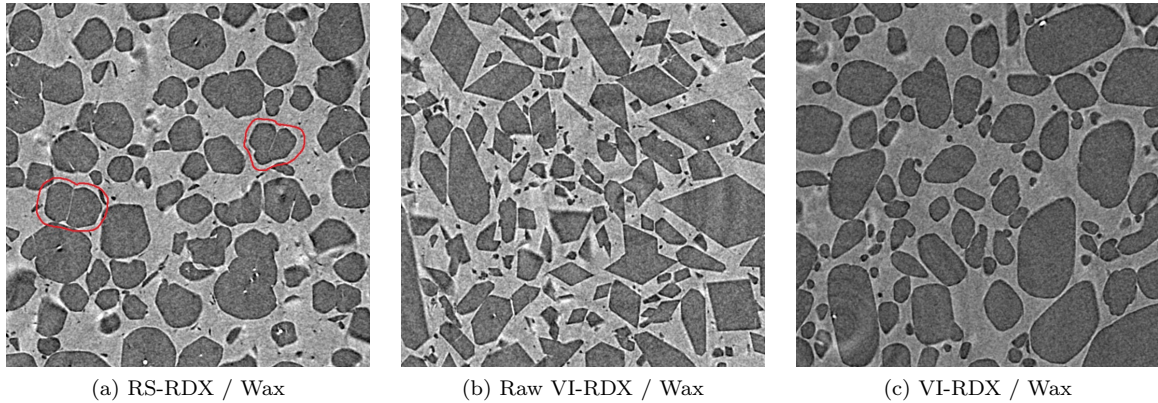


Figure 2: 600×600 voxels sections extracted from μ CT volumes for the three samples. Examples of RS-RDX twinned particles are highlighted on (a).

Image processing on micro-computed tomography images

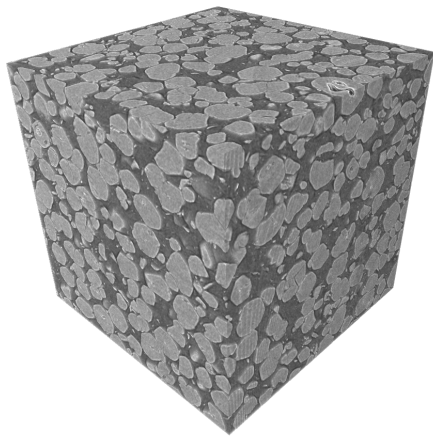
The microstructure of the three materials is imaged using the micro-computed tomography technique at the CEA Gramat. The μ CT is a Skyscan 1172. We obtained a large number of 2D slices of the material (Fig 2). The superposition of the slices gives access to the 3D microstructure. The samples imaged are cylindrical with a height of 10 mm and a radius of 5 mm. The resolution of acquisition for the VI-RDX based material is $3.54 \mu\text{m}/\text{voxel}$ and the resolution for the raw VI-RDX and the RS-RDX based materials is $3.67 \mu\text{m}/\text{voxel}$. One slice of each material is presented on the Figure 2. The grains of RDX appear in dark grey and the wax binder in light gray. The large white spots inside the grains are solvent inclusions or intra-granular porosities. The differences between the three types of RDX are clearly visible. We also notice that the RS-RDX grains tend to agglomerate. Some agglomerations of grains are in fact twinned grains.

The 3D volumes need to be filtered and segmented to characterize the microstructure. The filtering process aims to remove the noise without losing too much information on the boundaries of the grains. The segmentation consists of separating the binder from the RDX grains but also to individualize each grain of explosive. The two steps of filtering and segmentation are performed with a tool called SAMG (Automatic Segmentation of Granular Media) [12]. This software was developed at the Center for Mathematical Morphology, at MINES-ParisTech.

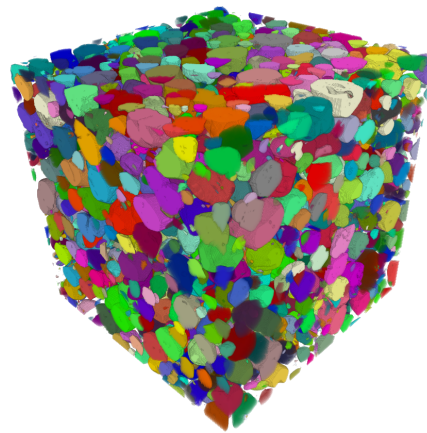
The filter applied to the 3D volumes is a recursive bilateral filter [13] implemented in SAMG. The parameters of the filter are chosen automatically based on two image analysis descriptors: the spatial covariance and the intensity distribution analysis. The spatial covariance helps to choose the standard deviation parameter of the filter. An intensity analysis of the 3D images allows to identify different classes (or phases) in the material. The intensity standard deviation parameter of the filter is based on the definition of the classes.

The next step is a segmentation with the watershed algorithm [14]. This process results in a coarse segmentation with numerous over-segmented grains which means that one grain has several labels. A process of over-segmentation correction is performed based on a geometric criterion [15]. The criterion quantifies the constriction between two adjacent labels. A low constriction reveals the presence of over-segmentation. The two labels describing the same grain are merged. A final step of manual correction is performed to correct the remaining segmentation errors. Between 10 minutes to 5 hours are necessary to correct a 1000^3 voxels volume with 6000 to 12000 grains. The time necessary to correct the RS-RDX based material is important because of the presence of twinned grains. The constriction between the labels of a twinned grain is too high to be corrected with the geometric criterion. One 1000^3 voxels volume is segmented for each material (Fig 3).

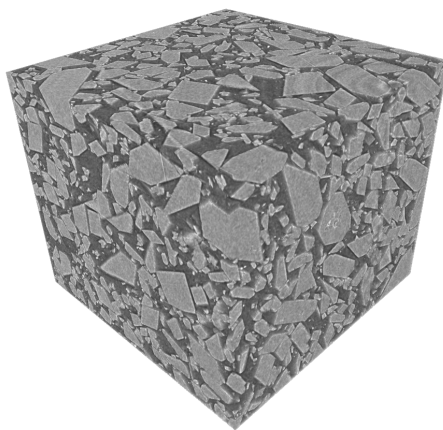
Each labelled grain is extracted to build a library of grains. The segmentations are validated by comparing the results with the results of experimental analysis. We compare three elements:



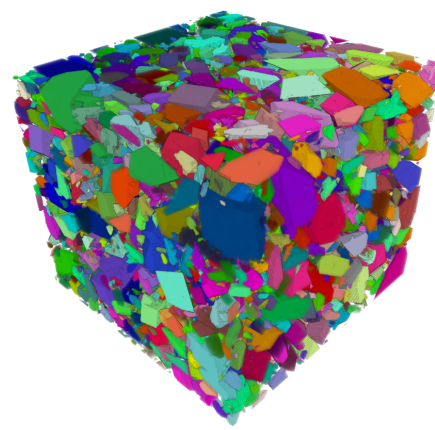
(a) μ CT RS-RDX/Wax



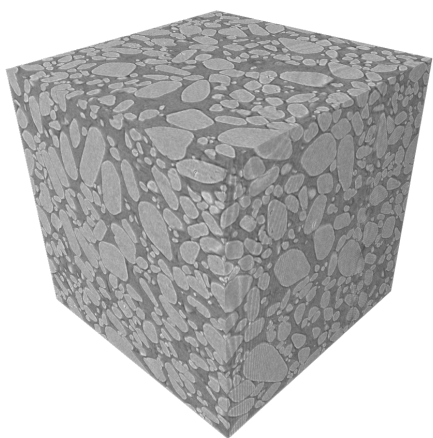
(b) segmented RS-RDX/Wax



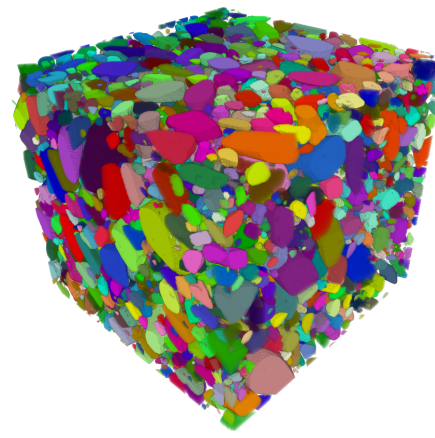
(c) μ CT raw VI-RDX/Wax



(d) segmented raw VI-RDX/Wax



(e) μ CT VI-RDX/Wax



(f) segmented VI-RDX/Wax

Figure 3: Micro-computed tomography volumes and the corresponding segmentations

Table 1: Characteristics of the segmented volumes

	RS-RDX/Wax	raw VI-RDX/Wax	VI-RDX/Wax
Number of grains	12719	6080	7178
Number of extracted grains	11159	4751	5677
Volume fraction of RDX (%)	52.8	54.6	54.1

- the theoretical volume fraction fixed by the formulation process and the final volume fraction of the segmented volumes,
- the experimental diameters distribution obtained with SLS (Static Light Scattering [16, 17]) and the distribution of the surface equivalent diameters of the extracted grains after the Miles-Lantuéjoul correction. The incomplete grains on the border of the volume are not considered. The probability for a large grain to be on the border of the volume is higher than for a small grain. This phenomenon introduces a bias in the size distribution of the extracted grains. To correct this bias, the Miles-Lantuéjoul correction is applied [18, 19]. This correction affects to each particle a probability to be fully enclosed in the volume. The initial number of grains and the number of extracted grains for each sample are presented on Table 1.
- the experimental bulk densities distribution obtained with the flotation method (ISL patent [20]) and the bulk densities distribution of the extracted grains.

Between the filtering and the segmentation process, a certain amount of voxels from the RDX grains are lost (very small grains and a few voxels on the boundaries of the grains). Instead of having a volume fraction of 56 % which corresponds to a 70 % weight fraction, we find a final volume fraction around 54 % for the three materials (Table 1). Both experimental diameters and bulk densities distributions are consistent with those obtained numerically from the RDX grains extracted of the three materials. The segmentations are considered reliable. Consequently: i) the 1000^3 voxels segmented volumes are considered as references for the generation of virtual microstructures ii) the library of extracted grains is used to generate virtual microstructures.

Characterization of the grains

Each grain is characterized by several descriptors. A fine characterization of the grains helps us to better understand the differences between the three type of RDX crystals. Moreover, in the generation of controlled virtual microstructures, adding a threshold on one or several descriptors allows one to select precisely some grains. We use the following descriptors:

- the volume and the reconstructed surface provided by the marching cube algorithm [21],
- the length, width and thickness of the minimal oriented bounded box of the grain,
- the diameters of the spheres with equal surface/volume as that of the grain and the mean diameter,
- the sphericity defined by Wadell [22], Bullard *et al.* [23], Delloro *et al.* [24] and Alshibli *et al.* [25],
- the angularity defined using the morphological operator of the opening,
- the number of intra-granular porosities and the volume of each porosity.

In the following section, we create virtual materials with prescribed distribution of sphericity and angularity. The definition used for the sphericity is the one given by Wadell [22]. The Wadell sphericity of a grain is defined as the ratio of the surface of a sphere with a diameter equal to the volume equivalent diameter, and the surface of the grain. This sphericity index is positive and bounded by 1 for a sphere.

The objective of the angularity index is to quantify the angularity of a particle. It is a particle shape descriptor. Several angularity indexes exist in the literature but are only defined for 2D projections of a 3D particle (see for exemple [26, 27, 28]). Few angularity indexes are defined on 3D particles [29, 30]. We developed a new angularity index defined by means of morphological openings which can be use on both 2D and 3D particles. The principle is to determine, for each point of the surface, the radius r of

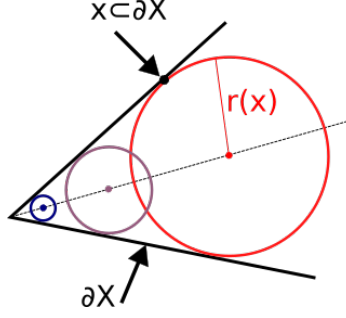


Figure 4: Principle of the determination of the tangent maximal inscribed sphere radius

the maximal tangent sphere inscribed in the particle (Fig. 4). This radius corresponds to the minimal radius of the spherical structuring element for which the voxel of the surface disappear. The radius r is normalized by the radius R of the maximal inscribed sphere in the grain. The normalization is necessary to have a measure of angularity independent of the size of the particle. Denote X the grain and ∂X its surface. The cumulative distribution function of the normalized radius $r_N = r/R$ of the maximal inscribed tangent sphere is defined by:

$$P(r_N, X) = P\{r_N(x) < \rho, x \in \partial X, \rho \in [0, 1]\} \quad (1)$$

The angularity index A (Eq. 2) is the integral of the previously introduced cumulated distribution:

$$A(x) = \int_0^1 P(r_N, X) dr_N \quad (2)$$

The angularity index is bounded by 0 for a sphere and 1 for a very angular shape like a straight line.

Generation of virtual microstructures

To better understand the role of each microstructural parameter, we create virtual microstructures. The algorithm to create the virtual microstructures is based on the RSA (Random Sequential Adsorption) principle [31]. Random positions are chosen until the current grain may be implanted, i.e. does not intersect any other grain. The RDX grains from the segmented μ CT volumes are extracted to create a library. Each grain of the library is characterized with several descriptors. By selecting the grains in the library depending on the value of the descriptors, we control the properties of the generated virtual microstructure. As a result, we are able to generate virtual microstructures representative of the real material but also to generate less realistic microstructures with specific grains from the library.

In our algorithm, the library of grains is divided into classes according to the size of the grains. We implant the grains sequentially starting from the class with the bigger grains and ending with the class which contains the smallest grains in order to have a multiscale microstructure and to be able to reach a 0.54 volume fraction of RDX. The generated sample volumes are periodic. In each class of grains, we only pick the particles we are interested in by fixing criteria on the properties of the grains. Once the grains which respect the criteria are identified in each class, they are randomly chosen and placed in the volume. For the first 20 grains, random positions are chosen until the grain is adsorbed. For the remaining grains, in case of intersections, the grain is moved in a previously chosen random direction. If the grain is not adsorbed after all the positions along the direction are tested, we choose a new random position. If after 50 new positions the grain is still not adsorbed, we select a new random grain in the class. These steps are repeated until the correct volume fraction from each class is reached and until the final volume fraction is reached.

Three microstructures of the VI-RDX/Wax material with different parameters are generated (Fig 5). We wish to obtain a grain volume fraction of 0.54 and the size distribution of RDX from the representative segmented material which is the μ CT segmented volume. To do so, we define 8 classes according to the volume of the grains and determine the volume of grains from each class necessary to be consistent with the reference volume of VI-RDX. For the first virtual microstructure, the grains are randomly

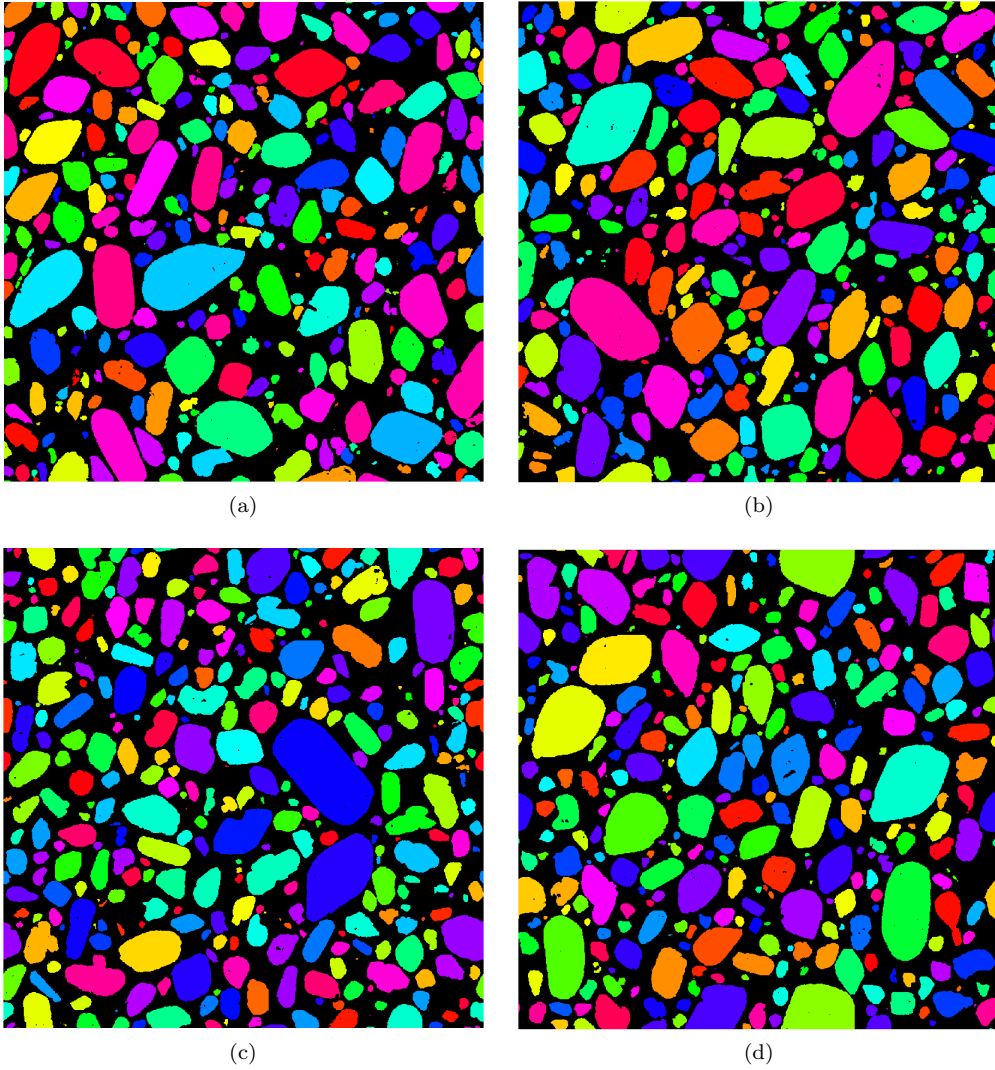


Figure 5: 1000×1000 voxels sections of VI-RDX/Wax of (a) segmented μ CT with labelled grains, (b) simulated microstructure representative of (a), (c) simulated microstructure containing grains with Wadell sphericity indexes > 0.88096 , (d) simulated microstructure containing grains with angularity indexes < 0.3105 .

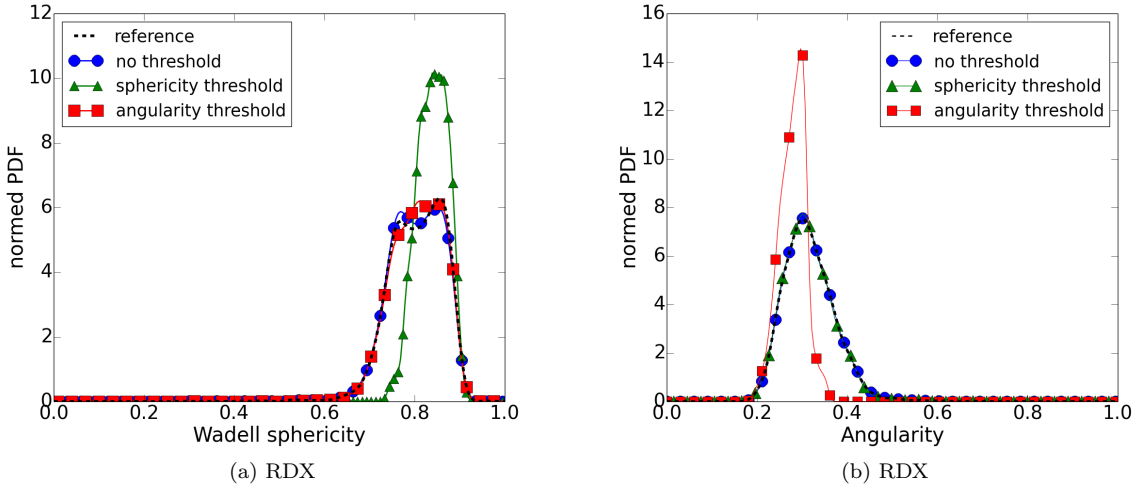


Figure 6: Comparison of the (a) sphericity and (b) angularity normed Probability Density Function (PDF) of the VI-RDX/Wax representative material and three VI-RDX/Wax virtual microstructures

chosen in each class i.e. there are no thresholds on the descriptors of the grains. In the second generated microstructure, only round-shaped grains are selected. The grains placed in the volume have a sphericity index higher than 0.8096. The third material is composed of grains with an angularity index under 0.3105. The threshold values for the sphericity and the angularity are the median values of all extracted grains of VI-RDX. But in certain classes, there are no grains which respect the angularity or sphericity criterion. In these classes, a new threshold value is determined such as 15 % of the particles of the class respect the new threshold. This method allows us to enforce the same size distribution for the grains in all generated microstructures and in the representative material. If for one class, less than 15 % of the particles of the class respect the initial threshold, a new 15 % threshold is also determined. This process avoid to have only one grain in the class and to find it numerous times in the volume.

Slices extracted from the μ CT segmented volume and from the three virtual materials are presented on Figure 5. The four volumes seem visually similar. The angularity indexes distributions and the Wadell sphericity indexes distributions of the RDX grains are plotted to quantify the effect of the criterion on the microstructure (Fig. 6). The material with no criteria is consistent with the representative volume for both sphericity and angularity. The sphericity controlled microstructure respects the angularity distribution of the representative material but the sphericity distribution is truncated because of the threshold we applied. Respectively, the angularity controlled microstructure respects the sphericity distribution of the representative material but the angularity distribution is truncated. These results show that we are able to slightly modify one parameter of the microstructure without affecting other parameters.

Validation of the virtual materials

The generated microstructures have to be representative of the real material by respecting the RDX sizes distribution, spatial distribution and volume fraction. The validation of the virtual microstructures is made with the comparison of two descriptors for the representative and virtual volumes: i) the morphological granulometry of the grains and the binder and ii) the spatial covariance.

The segmented volumes are converted into binary images (RDX grains/wax binder) so that we can compute the granulometry of each phase (Fig. 7). The determination of the granulometric curve is obtained with the residues of successive morphological openings operations defined as:

$$F_n(X) = 1 - \frac{Mes(\gamma_n(X))}{Mes(\gamma_0(X))} \quad (3)$$

where $\gamma_n(X)$ is the opening of size n on the subset X [32] and $Mes(X)$ is the Lebesgue measure (here

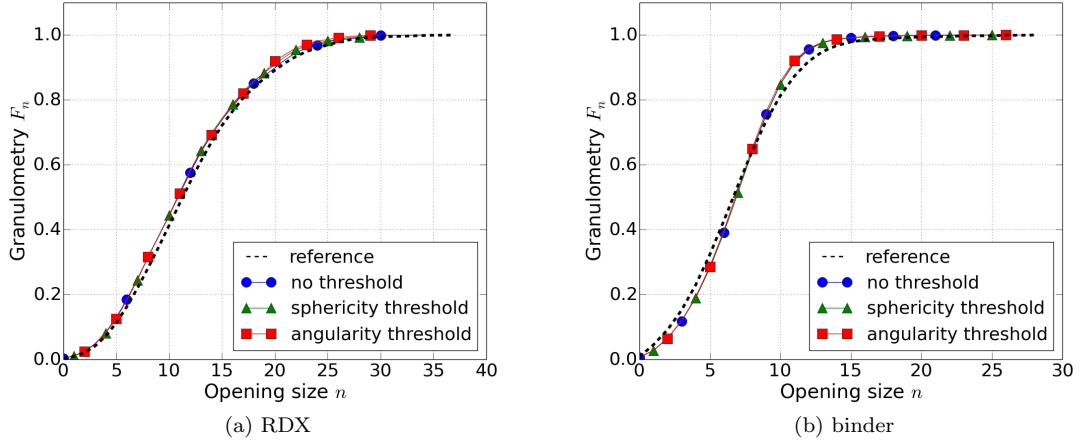


Figure 7: Granulometry of (a) the RDX grains and (b) the binder of the VI-RDX/Wax representative material and three VI-RDX/Wax virtual microstructures

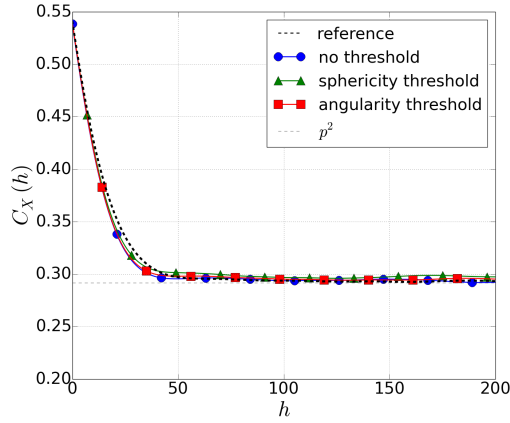


Figure 8: Comparison of the spatial covariance of the VI-RDX/Wax representative material and the three VI-RDX/Wax virtual microstructures

the volume). X is the phase we measure the granulometry of, i.e. the RDX or the binder.

The granulometric curves of the four materials are similar. This indicates that 8 classes are sufficient to reproduce the sizes distribution of the representative material. The granulometry of the binder is not a parameter directly controlled in the software developed to generate virtual microstructures. Nonetheless, the binder granulometry of the four materials are nearly identical. This allows us to conclude that the generated microstructures respect the granulometry of the μ CT segmented volume.

The second verification is the spatial covariance [33]. The spatial covariance $C_X(h)$ is the probability that two points x and $x + h$ lie on the same phase (Eq. (4)). As a consequence, $C_X(0)$ corresponds to the volume fraction p of the phase X . The covariance reaches a plateau for h_∞ which is equal to p^2 .

$$C_X(h) = \{x \in X, x + h \in X\} \quad (4)$$

The covariance is computed for the four materials along the same direction. First, we notice that we are able to reach the 0.54 RDX volume fraction as $C(0)$ is equal to 0.54 for the three generated microstructures. The spatial covariance of the four microstructures are similar. We conclude that the covariance of the virtual volumes respect the one of the representative volume.

Finally, we consider that the three virtual microstructures are representative of the real microstructure.

Conclusion

Three materials composed of RDX and wax (70/30 in weight) with different microstructures are imaged with μ CT. We successfully segmented a large volume of 1000^3 voxels for each material with the software SAMG. The labelled grains are extracted and characterized by several descriptors to form a library of grains. The extracted grains are implanted in a virtual volume with the RSA method.

With this process, we are able to generate microstructures representative of the real material. The virtual microstructures are validated by comparing the morphological granulometry of RDX grains and binder in the μ CT volume and simulated microstructures, as well as the spatial covariance. The generation of representative microstructures allow us to work on a large number of independant volumes. With the RSA method and the library of grains, we are also able to generate controlled microstructures where one microstructural parameter at a time is modified. It allows us to uncorrelate parameters and to, in future work, better understand the role of one microstructural parameter on the sensitivity to shock of energetic materials.

Future work

The generated microstructures will be used in quasistatic and dynamic simulations. Thermoelastic calculations under hydrostatic loading conditions are solved with the FFT method [34]. The microstructures are also used in eulerian mesoscale simulations of a shockwave propagating in the material with the hydrocode OURANOS [35]. Different indicators like the maximal pressure, maximal strength and the density of hot spots will be determined. The comparison of these indicators between the different virtual materials will help us to better understand the role of microstructural parameters on the sensitivity of an explosive. Ideally, only one microstructural parameter varies from one virtual material to another so we have a direct information on the influence of the parameter on the sensitivity.

Acknowledgements

This work was partly supported by the French General Directorate for Armament (DGA) of the Ministry of the Armed Forces. The authors are also grateful to P. Rey (CEA Gramat) for its technical contribution to this project.

References

- [1] F. P. Bowden and A. D. Yoffe. *Initiation and growth of explosion in liquids and solids*. Cambridge University Press, 1952.
- [2] A. C. van der Steen, H. J. Verbeek, and J. J. Meulenbrugge. Influence of RDX crystal shape on the shock sensitivity of PBXs. In *Ninth Symposium (International) on Detonation*, volume 1, 1989.
- [3] H. Moulard, A. Delclos, and J. W. Kury. The Effects of RDX Particle Size on the Shock Sensitivity of Cast PBX Formulations. In *Eight Symposium (International) on Detonation*, 1985.
- [4] L. Borne. Influence of intragranular cavities of RDX particles batches on the sensitivity of cast wax bonded explosives. In *Tenth Symposium (International) on Detonation*, pages 286–293, 1993.
- [5] L. Borne. Explosive crystal microstructure and shock-sensitivity of cast formulations. In *Eleventh Symposium (International) on Detonation*, 1998.
- [6] L. Baillou, J.M. Dartyge, C. Spyckerelle, and J. Mala. Influence of crystal defects on sensitivity of explosives. In *Tenth Symposium (International) on Detonation*, pages 816–823, 1993.
- [7] A. W. Campbell, W. C. Davis, J. B. Ramsay, and J. R. Travis. Shock initiation of solid explosives. *The Physics of Fluids*, 4(4):511–521, 1961.
- [8] R. Menikoff. Pore collapse and hot spots in HMX. In *AIP Conference Proceedings*, volume 706, pages 393–396, 2004.

- [9] A. Barua, S. Kim, Y. Horie, and M. Zhou. Ignition criterion for heterogeneous energetic materials based on hotspot size-temperature threshold. *Journal of Applied Physics*, 113(6):064906, February 2013.
- [10] R. Menikoff. Hot spot formation from shock reflections. *Shock Waves*, 21(2):141–148, April 2011.
- [11] L. Borne. Particles of explosive of low sensitivity to shock and associated treatment process, June 2006. US 8,747,581 B2.
- [12] T. Chabardès. *Segmentation Automatique de Matériaux Granulaires*. PhD thesis, Mines Paristech, Fontainebleau, May 2018.
- [13] Q. Yang. Recursive Bilateral Filtering. In *Computer Vision – ECCV 2012*, Lecture Notes in Computer Science, pages 399–413. Springer, Berlin, Heidelberg, October 2012.
- [14] Serge Beucher. Watershed, Hierarchical Segmentation and Waterfall Algorithm. In Max A. Viergever, Jean Serra, and Pierre Soille, editors, *Mathematical Morphology and Its Applications to Image Processing*, volume 2, pages 69–76. Springer Netherlands, Dordrecht, 1994.
- [15] T. Chabardès, P. Dokládal, M. Faessel, and M. Bilodeau. An affinity score for grains merging and touching grains separation. In *13th International Symposium on Mathematical Morphology*, volume 10225, pages 423–434, Fontainebleau, France, May 2017.
- [16] P. Debye. Molecular-weight determination by light scattering. *The Journal of Physical and Colloid Chemistry*, 51(1):18–32, 1947.
- [17] B. H. Zimm. The scattering of light and the radial distribution function of high polymer solutions. *The Journal of Chemical Physics*, 16(12):1093–1099, 1948.
- [18] R. E. Miles. On The Elimination of Edges Effects in Planar Sampling. In *Harding EF, Kendall DG*, pages 228–247, New York, 1974. Stochastic Geometry.
- [19] C. Lantuejoul. On the estimation of mean values in individual of particles. *Microscopica Acta*, 5(266):73, 1980.
- [20] L. Borne and J.-L. Patedoye. Device for measuring the density of particles by flotation, June 2009. US 7,607,341 B2.
- [21] W. E. Lorensen and H. E. Cline. Marching Cubes: A high resolution 3D surface construction algorithm. In *Proceedings of the 14th Annual Conference on Computer Graphics and Interactive Techniques*, pages 163–169. ACM, 1987.
- [22] H. Wadell. Sphericity and roundness of rock particles. *The Journal of Geology*, 41(3):310–331, 1933.
- [23] J. W. Bullard and E. J. Garboczi. Defining shape measures for 3D star-shaped particles: Sphericity, roundness, and dimensions. *Powder Technology*, 249:241–252, November 2013.
- [24] F. Delloro. *Méthodes morphologique et par éléments finis combinées pour une nouvelle approche de la modélisation 3D du dépôt par projection dynamique par gaz froid (" cold spray ")*. PhD thesis, Ecole Nationale Supérieure des Mines de Paris, July 2015.
- [25] K. A. Alshibli, A. M. Druckrey, R. I. Al-Raoush, T. Weiskittel, and N. V. Lavrik. Quantifying morphology of sands using 3D imaging. *Journal of Materials in Civil Engineering*, 27(10), October 2015.
- [26] B. Sukumaran and A. K. Ashmawy. Quantitative characterisation of the geometry of discrete particles. *Géotechnique*, 51:619–627, September 2001.
- [27] T. Al-Rousan, E. Masad, E. Tutumluer, and T. Pan. Evaluation of image analysis techniques for quantifying aggregate shape characteristics. *Construction and Building Materials*, 21:978–990, May 2007.
- [28] S. Tafesse, F. Robison, M. Joanne, W. Sun, and F. Bergholm. Evaluation of image analysis methods used for quantification of particle angularity. *Sedimentology*, 60:1100–1110, June 2013.

- [29] X. Yang, S. Chen, and Z. You. 3D Voxel-Based Approach to Quantify Aggregate Angularity and Surface Texture. *Journal of Materials in Civil Engineering*, 29:04017031, July 2017.
- [30] B. Zhao and J. Wang. 3D quantitative shape analysis on form, roundness, and compactness with μ CT. *Powder Technology*, 291:262–275, April 2016.
- [31] J. Feder. Random sequential adsorption. *Journal of Theoretical Biology*, 87(2):237 – 254, 1980.
- [32] J. Serra. *Image Analysis and Mathematical Morphology*. Academic Press, Inc., Orlando, FL, USA, 1982.
- [33] G. Matheron. *Random Sets and Integral Geometry*. Wiley, 1974.
- [34] H. Moulinec and P. Suquet. A FFT-Based numerical method for computing the mechanical properties of composites from images of their microstructures. In *IUTAM Symposium on Microstructure-Property Interactions in Composite Materials*, Solid Mechanics and Its Applications, pages 235–246. Springer, Dordrecht, 1995.
- [35] H. Jourden, J. M. Sibeaud, and M. M. Adamczewski. Logiciel ouranos : présentation générale et utilisation en détonique. *Revue Scientifique et Technique de Défense*, 4:51–58, 1995.